COMMUNICATION

Optimising Molecular Rotors to AIE Fluorophores for Mitochondria Uptake and Retention

Received 00th January 20xx,
Accepted 00th January 20xx

DOI: 10.1039/x0xx00000x

Tze Cin OwYong,[a,b] Siyang Ding,[b] Na Wu,[a] Thomas Fellowes,[a] Sijie Chen,[c] Jonathan M. White,[a] Wallace W. H. Wong,*[a] and Yuning Hong*[b]

Molecular rotors exhibit fluorescence enhancement in a confined environment and thus have been used extensively in biological imaging. However, many typical molecular rotors suffer from small Stokes shift and self-aggregation caused quenching. In this work, we have synthesised a series of red emissive molecular rotors based on cationic α-cyanostilbene. Profoundly enhanced aggregation-induced emission (AIE) properties and greatly widened Stokes shifts can be achieved by molecular engineering. With excellent specificity to stain mitochondria, we further demonstrate the alternation of substituents on the pyridinium of the dyes can be a simple approach to achieve cell uptake and retention upon fixation.

Fluorescent molecules have been shown to be powerful and crucial tools in many fields with biology being one of them. A class of fluorophores that have been well used are the molecular rotors.[1-3] The general structures of these fluorophores are conjugated molecules containing a structure that can undergo intramolecular rotations. When free intramolecular rotation of the dye occurs, a dye excited by light can undergo relaxation to the ground state through nonradiative pathways, and thus there is low fluorescence intensity and short fluorescence lifetime. Upon restriction of intramolecular rotation (RIR) by viscosity or steric effects, the nonradiative pathways are inhibited, thus resulting in an enhancement of fluorescence intensity and a prolonged fluorescence lifetime.[4] However, some of the fluorescent molecular rotors suffer from self-aggregation caused quenching effect when the concentration is high.[5-6] On the other hand, aggregation-induced emission (AIE) is a term which describes

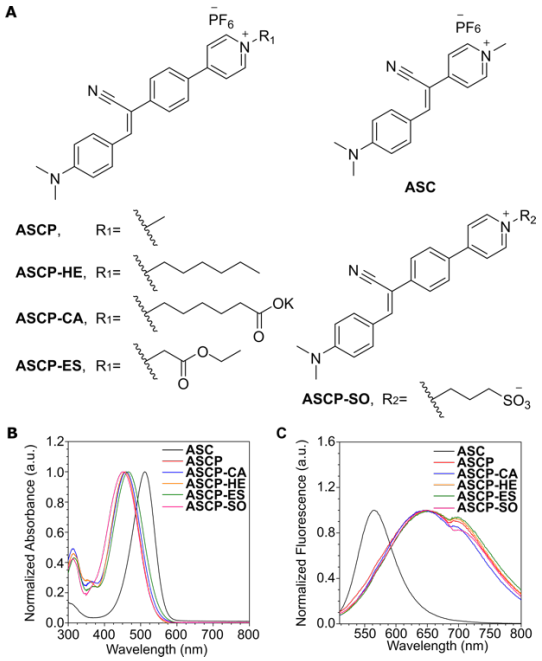

Figure 1 (A) Chemical structures of dyes in this study. Comparison of (B) absorption and (C) emission spectra of all dyes measured in iPrOH. 488nm excitation wavelength was used for fluorescence measurements. 10 μM dye concentration was used for all measurements. Note that the dip in fluorescence intensity was due to the change of filter.

the phenomenon that the dye molecules shows enhanced emission in the aggregated states. Restriction of the intramolecular motion, which includes not only the intramolecular rotation but also other types of internal motions, is usually used for the explanation of the AIE mechanism. AIE-active molecules, due to their chemical structure, often twisted, have greater difficulties in packing closely or engaging in π-π stacking interactions, and thus exhibit strong fluorescence at high concentration or in aggregate states.[7-8] Most of the AIE-active molecules, including the typical tetraphenylethene and silole, possess rotatable phenyl rings. However, not all the AIE molecules are molecular rotors, examples of which include some recently reported AIE molecules that do not have any rotors.[9-10]

[a] *ARC Centre of Excellence in Exciton Science, School of Chemistry, Bio21 Institute, The University of Melbourne, Parkville, VIC 3010 Australia*
Email: wwhwong@unimelb.edu.au
[b] *Department of Chemistry and Physics, La Trobe Institute for Molecular Science, La Trobe University, Melbourne, VIC 3086, Australia*
Email: y.hong@latrobe.edu.au
[c] Ming Wai Lau Centre for Reparative Medicine, Karolinska Institutet, Hong Kong
† Footnotes relating to the title and/or authors should appear here.
Electronic Supplementary Information (ESI) available: materials and methods, synthesis procedure, photophysical studies, X-ray crystallography, DFT calculation, cell viability and imaging and NMR spectra. See DOI: 10.1039/x0xx00000x

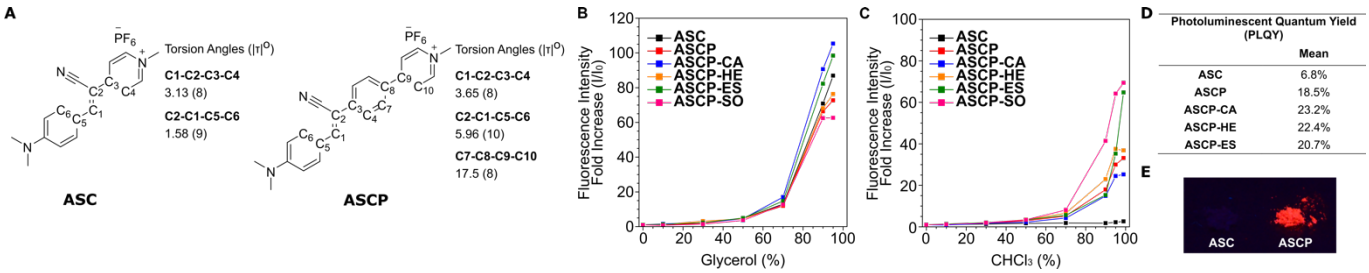

Figure 2 Molecular rotor and AIE properties of the dye series. (A) Torsional angles of **ASC** and **ASCP** measured from crystallography experiments. (B) Fold of increase in fluorescence intensity of dyes in water and glycerol mixtures with increasing fraction of glycerol from 0, 10, 30, 50, 70, 90, 95 vol%. (C) Fold of increase in fluorescence intensity of dyes in DMSO and chloroform ($CHCl_3$) mixtures with increasing fraction of $CHCl_3$ from 0, 10, 30, 50, 70, 90, 95, and 99 vol%. (D) Absolute photoluminescent quantum yield (PLQY) of dyes in PMMA matrix (2% weight ratio). Note that due to the poor solubility of **ASCP-SO** in acetone, its PLQY was not measured. (E) Photograph of **ASC** and **ASCP** in the solid state was obtained under 365 nm UV lamp excitation. Plots were obtained by taking fluorescence emission intensity value at 575 nm for **ASC** and 650 nm for **ASCP** derivatives. 10 μM dye concentration was used for dye self-aggregate and viscosity experiments. 488 nm excitation wavelength was used for all measurements.

Given the broad research interest in both fluorescent molecular rotors and AIE molecules, here, we report the study of a cationic α-cyanostilbene, namely **ASC**, the reported compound **ASCP**, and its new derivatives, to decipher the differences between these two types of fluorophores (Figure 1A).[11] All these molecules possess molecular rotor type of photophysical behaviours. Compared with **ASC**, addition of a phenyl ring bridge endows enhanced AIE property to the **ASCP** series. With large Stokes shift and emission in the red region, we explore the application of **ASCP** series for cell imaging.

As a key organelle in eukaryotic cells, mitochondria are involved in production of ATP, the currency of energy in cells.[12] Apart from the crucial process of providing energy, mitochondria are involved with reactive oxygen species (ROS), participate in transcription regulation and govern cell death.[13-15] Furthermore, the dynamics and morphology of mitochondria also have been implicated in disease and affected by a set of proteins, with mutations leading to diseases including neurodegeneration.[16-17] Further development and improvement on current fluorescent mitochondria stains would give insight for monitoring these processes.

In many biological applications, real-time monitoring of mitochondria morphological changes is of great interest.[18-19] With the aid of fluorescent molecular rotors, even local viscosity of mitochondria can be measured.[20-21] On the other hand, cell fixation is commonly used for the ease of sample handling and preservation as well as for further antibody labelling of a particular target protein. Although many of these stains work in live cell conditions, retention of their signal after fixation is usually achieved by using a covalent strategy as seen in the commercial MitoTracker dyes. Covalent labelling, however, could potentially affect the dynamics when used in live cells.[22-24] In this work, we demonstrate that molecular structure plays a large role in cellular uptake and retention. By altering the substituent on the pyridinium moiety, we improve the cell uptake and retention of **ASCP**, demonstrating a noncovalent strategy for labelling mitochondria in both fixed and live cells.

ASC, **ASCP** and derivatives were synthesised according to the synthetic routes shown in Scheme S1-3 in the supplementary information. All synthesised products were characterized by ^1H, ^{13}C NMR and high-resolution mass spectrometry (refer to ESI). The structures of **ASC** and **ASCP** were further confirmed by single crystal X-ray crystallography (Figure S1, Table S1-2).

UV-vis absorption spectra of **ASC**, **ASCP** and derivatives in different solvents were measured. The results showed that the smaller **ASC** has an absorption maximum ranging from 504–530 nm and exhibits minimal shifts with regards to solvent dielectric constants (Figure 1B, S2A, Table S3). On the other hand, **ASCP** has an absorbance maximum in the range of 411–497 nm and a small red shift in the absorbance maximum in less polar, lower dielectric constant solvent (Figure 1B, S2B). The **ASCP** derivatives have very similar absorption characteristics as **ASCP** (Figure 1B and S2B-F, Table S3).

The emission spectra of **ASC** were centred at around 560 nm in various solvents with minimal changes in the wavelength and some differences in fluorescence intensity (Figure 1C, S3A). The only exception was in toluene where a second emission peak at around 715 nm was observed. For **ASCP** and derivatives, we observed red-shifted spectra in a more polar, higher dielectric constant solvent like DMSO, as compared to nonpolar solvents such as chloroform (Figure S3B-F). The largest fluorescence intensity was from chloroform, which we attributed to the poor solubility of dyes in chloroform and subsequent AIE affects (*vide infra* Figure 2C). While the main emission peaks of **ASCP** and derivates are red-shifted to 650 nm, their emission spectra are also broader compared to **ASC** (Figure 1C). When comparing the Stokes shift of the dyes, **ASC** possesses a much smaller Stokes shift (53 nm) in comparison to **ASCP** derivatives with Stokes shift in the range of 170–195 nm (Figure 1B-C, Table S4).

From the absorption spectra in Figure 1B, we can estimate that **ASC** has better π conjugation than **ASCP** and derivatives. The X-ray crystallography data further confirmed that **ASC** has a more planar conformation than **ASCP**, with smaller torsional angles (**ASC**: 1.58–3.13°; **ASCP**: 3.65 to 5.96°) between the aromatic rings and the central double bond. Pyridinium groups of **ASCP** and derivatives had a larger torsion angle of 17.5° (Figure 2A, S4). The improved conjugation could potentially confine the conformation to a larger extent as seen in the sharper peaks observed in **ASC** compared to those of **ASCP** (Table S4 and Figure 1C, S3A).[8] We speculated that the second emission peak at 715 nm for **ASC** in toluene originated from the formation of excimer when dye molecules aggregate (Figure S3A). This peak became predominant in crystalline **ASC** (Figure

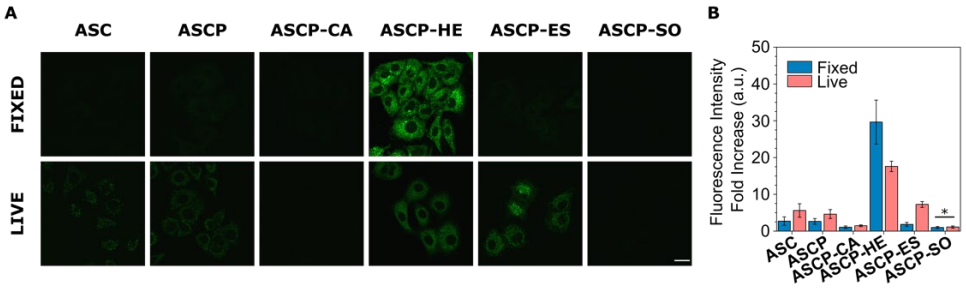

Figure 3 Cell uptake and retention of dyes. (A) Confocal images of dye staining A549 cells with (fixed) and without fixation (live). (B) Fluorescence intensity analysis of imaged cells. Unless specified in the figure, comparison between respective fixed and live fluorescence intensities for each respective dye had $p < 0.0001$ significance. *= $p < 0.05$. mean ± sd. Scale Bar, 20μm. For **ASCP** and derivatives (excitation: 488 nm; emission: 615–650 nm), **ASC** (excitation: 488 nm; emission 520–560 nm).

S10). In the case of **ASCP**, we did not observe a distinct peak at longer wavelength under all conditions including the crystalline state and in toluene. These results suggest the more planar structure of **ASC** could facilitate stronger intermolecular interaction, which is reduced in **ASCP** possibly due to twisted configuration. DFT calculations showed a clearer distinction of the HOMO and LUMO electron density distributions of **ASCP** with HOMO mostly localized on the electron donor dimethylamine moiety while the LUMO was more centred on the positively charged electron withdrawing pyridinium (Figure S5). For **ASC**, similar HOMO and LUMO distributions were found but less distinguishable. This is consistent with our observation that the fluorescence of **ASC** is less sensitive to solvent polarity than that of **ASCP** (Figure S3). The electrostatic potential data from X-ray diffraction experiment further supported this observation of HOMO-LUMO distribution for **ASC** (Figure S6).

We then proceeded to characterize the molecular rotor and AIE nature of the dyes. To induce restriction of intramolecular motions, we measured the viscosity effect by increasing glycerol percentage. Our results showed that above 50% glycerol concentration, all dyes had an increases of fluorescence intensity. Maximum dye intensity was observed at the highest glycerol concentration measured (95%) (Figure 2B, S8, Table S6). A linear relationship was found between the fluorescence intensity of **ASC**, **ASCP** and **ASCP-HE** in a logarithm scale and percentage of glycerol, implying the potential of using the dye fluorescence to measure viscosity in the media (Figure S9). These results showed that all dyes possess molecular rotor behaviour, where rigidification of the molecule results in the fluorescence intensity enhancement.

To study the self-aggregation effect on fluorescence, we measured the emission intensity of dyes in DMSO/chloroform ($CHCl_3$) with increased fraction of chloroform, a poor solvent for the dyes, that induce dye aggregation (Table S7). For the **ASCP** series, there were large fluorescence intensity enhancements beyond 70% chloroform. Most **ASCP** dyes achieved maximum fluorescence intensity at 99% chloroform with fluorescence fold increases ranging from 25–82 fold. For the smaller **ASC**, we only observed a minimal increase in fluorescence intensity at 99% chloroform with modest 2.6 fold increase (Figure 2C, S7, Table S6-7). To further confirm the results, we measured the absolute photo-luminescence quantum yields (PLQY) of **ASC** and **ASCP** in different conditions. The PLQY recorded in DMSO and chloroform is in line with our observation of fluorescence intensity (Table S6 vs Figure 2C). In poly(methyl methacrylate) (PMMA) thin films with 2% dye doping, all dyes had their highest PLQY. We found that the **ASCP** series had a PLQY, in the range of 19–23%, while **ASC** was recorded at ca. 7% (Figure 2E, Table S5). Collectively, our results demonstrated that with a more twisted structure, the tendency of strong intermolecular interaction such as π-π stacking in **ASCP** is much lower and thus exhibits a stronger AIE characteristic compared to **ASC**.

We further investigated the effect of the substituents on the pyridinium unit of **ASCP** on cell uptake and retention. Firstly, we evaluated the cytotoxicity of the dyes by using the AlamarBlue™ assay, which demonstrated all dyes had low to moderate cytotoxicity when the concentration is below 5 μM even after treatment for 24 h (Figure S11). Our first attempt at cell staining involved treating live A549 cells with dyes at the desired concentration followed by fixation with 4% paraformaldehyde (PFA). Confocal imaging shown that among **ASC** and **ASCP** and derivatives, only **ASCP-HE** with a hexyl chain showed strong fluorescence staining, mitochondria-like pattern in the cells under 488 nm laser excitation (Figure 3A).

In order to determine the reasons for the lack of staining for most of the dyes, live cell imaging without PFA fixation was carried out under the same imaging conditions (Figure 3A). While **ASCP-HE** and **ASCP-ES** gave the highest fluorescence intensity in the live cells, the response for **ASC**, **ASCP** and **ASCP-ES** was improved, and mitochondria-like staining patterns were also observed. In the case of **ASCP-HE**, we observed good staining with appreciable intensity in both live and fixed cells. For zwitterionic **ASCP-CA** and **ASCP-SO**, minimal cell uptake was observed in either live or fixed conditions. Further analysis of the fluorescence intensity of stained compartments showed **ASC**, **ASCP** and **ASCP-ES** all had higher fluorescence intensities in live cells, implying that fixation of the cells affects the retention of these dyes (Figure 3B). These results suggested that a net positive charge would assist in membrane permeability and thus increase the cell uptake of the dye. Meanwhile, fluorophore lipophilicity plays an important role in not only cell uptake but also retention of non-covalent dye molecules in cells, as seen in **ASCP-HE** with a hydrophobic non-charged hexyl chain. Therefore, the lack of staining for the dyes except **ASCP-HE** in fixed cells could arise for two reasons, or a combination of both. The first was the lack of penetration of dye before fixation. The second, was low retention of dye in cells upon fixation.

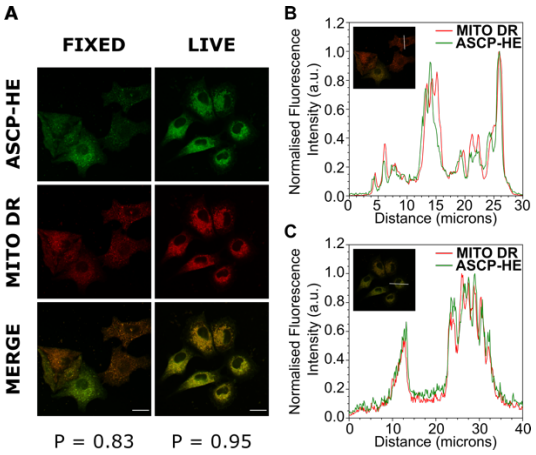

Figure 4 Mitochondrial colocalization. (A) Confocal images of intracellular distribution of **ASCP-HE** stained A549 cells with (fixed) and without fixation (live). A549 cells were stained with **ASCP-HE** and counterstained with MitoTracker™ Deep Red FM (MITO DR) for visualisation of mitochondria. Pearson correlation values (P) were calculated. (B,C) Fluorescence intensity kymograph analysis for colocalization of intracellular distribution of **ASCP-HE** stained (B) fixed and (C) live A549 cells. Cells were stained using 5 μM of **ASCP-HE** and 500 nM of MITO DR. Scale Bar, 20μm. For ASCP-HE (excitation: 488 nm; emission: 615–650 nm), MITO DR (excitation: 633 nm; emission 660–700 nm).

With the promising results from **ASCP-HE**, we carried out co-localization experiments to confirm the staining patterns. Dye crosstalk experiments verified that there was no signal bleedthrough from the mitochondria stain, MitoTracker™ Deep Red (**MITO DR**) in our dye channel (Figure S12). **MITO-DR** carries a reactive benzyl chloride to covalently label on biomolecules and thus works in both live and fixed cells. The staining patterns for **ASCP-HE** were colocalized with **MITO-DR**, with Pearson correlation factor (P) of 0.83 (Figure 4). **ASCP-HE** was further confirmed to localize in fixed cells by obtaining z-stack images (Figure S13). Subsequent live cell colocalisation experiments were then carried out, which showed the staining patterns of **ASCP-HE** was greatly colocalized with **MITO DR** with P of 0.95 (Figure 4).[25] In addition to the non-covalent nature, **ASCP-HE** also possesses large Stokes shift compared to **MITO DR**, which would be favourable in the imaging setup.

In summary, we have designed and synthesised a series of cationic α-cyanostilbene derivatives, including **ASC**, **ASCP** and its derivatives. By comparing the photophysical behaviours of **ASC** and **ASCP**, we demonstrated the correlation between the extent of conjugation and structure rigidity. We further studied their fluorescence response upon rigidification in solid film, upon aggregation and in high viscosity. Whereas all of the molecules possess molecular rotor like behaviour, the addition of a phenyl bridge to **ASC** leads to a remarkable enhancement of the AIE effect with large Stokes shift. These red-emitting dyes show specificity to mitochondria. Upon changing the substituent on the pyridinium of **ASCP**, we demonstrated the crucial role of lipophilicity in cell uptake and developed a simple, non-covalent strategy to achieve excellent retention upon cell fixation. Such strategy could be further applied in other organelle targeting imaging agents.

Conflicts of interest

There are no conflicts to declare.

Acknowledgements

We thank LIMS Bioimaging Platform, La Trobe University for the access to confocal microscope and the Bio21 Mass Spectrometry and Proteomics Facility for technical support and access to mass spectrometers. This work was supported by grants to Y.H. (Australian Research Council DE170100058, Rebecca L. Cooper Medical Research Foundation PG2018043, and Australia-China Science and Research Fund-Joint Research Centre for Personal Health Technologies ACSRF65777) and WWHW (Australian Research Council CE170100026).

Notes and references

1 R. O. Loutfy, B. A. Arnold, *J. Phys. Chem.* 1982, **86**, 4205-4211.
2 J. Sutharsan, D. Lichlyter, N. E. Wright, M. Dakanali, M. A. Haidekker, E. A. Theodorakis, *Tetrahedron.* 2010, **66**, 2582-2588.
3 M. K. Kuimova, *Phys. Chem. Chem. Phys.* 2012, **14**, 12671-12686.
4 Z. Yang, J. Cao, Y. He, J. H. Yang, T. Kim, X. Peng, J. S. Kim, *Chem. Soc. Rev.* 2014, **43**, 4563-4601.
5 F. Würthner, T. E. Kaiser, C. R. Saha-Möller, *Angew. Chem. Int. Edit.* 2011, **50**, 3376-3410.
6 Z. Liu, Z. Jiang, M. Yan, X. Wang, *Front. Chem.* 2019, **7**, 712.
7 Y. Hong, J. W. Y. Lam, B. Z. Tang, *Chem. Commun.* 2009, **29**, 4332-4353.
8 Y. Hong, J. W. Y. Lam, B. Z. Tang, *Chem. Soc. Rev.* 2011, **40**, 5361-5388.
9 Y. Gu, Z. Zhao, H. Su, P. Zhang, J. Liu, G. Niu, S. Li, Z. Wang, R. T. K. Kwok, X.-L. Ni, J. Sun, A. Qin, J. W. Y. Lam, B. Z. Tang, *Chem. Sci.* 2018, **9**, 6497-6502.
10 F. Bu, R. Duan, Y. Xie, Y. Yi, Q. Peng, R. Hu, A. Qin, Z. Zhao, B. Z. Tang, *Angew. Chem. Int. Edit.* 2015, **54**, 14492-14497.
11 C. Y. Y. Yu, W. Zhang, R. T. K. Kwok, C. W. T. Leung, J. W. Y. Lam, B. Z. Tang, *J. Mater. Chem. B.* 2016, **4**, 2614-2619.
12 Y.-L. P. Ow, D. R. Green, Z. Hao, T. W. Mak, *Nat. Rev. Mol. Cell Biol.* 2008, **9**, 532-542.
13 D. E. Handy, J. Loscalzo, *Antioxid. Redox Sign.* 2011, **16**, 1323-1367.
14 G. Barshad, S. Marom, T. Cohen, D. Mishmar, *Trends Genet.* 2018, **34**, 682-692.
15 C. Wang, R. J. Youle, *Annu. Rev. Genet.* 2009, **43**, 95-118.
16 M. Filosto, M. Scarpelli, M. S. Cotelli, V. Vielmi, A. Todeschini, V. Gregorelli, P. Tonin, G. Tomelleri, A. Padovani, *J. Neurol.* 2011, **258**, 1763-1774.
17 A. Johri, M. F. Beal, *J. Pharmacol. Exp. Ther.* 2012, **342**, 619.
18 N. Zhao, S. Chen, Y. Hong, B. Z. Tang, *Chem. Commun.* **2015**, 51, 13599-13602.
19 C.Y.-W. Lo, S. Chen, S. J. Creed, M. Kang, N. Zhao, B. Z. Tang, K. D. Elgass, *Sci. Rep.* 2016, **6**, 30855.
20 D. Su, C. L. Teoh, N. Gao, Q.-H. Xu, Y. T. Chang, *Sensors* 2016, **16**, 1397.
21 X. Song, N. Li, C. Wang, Y. Xiao, *J. Mater. Chem. B* 2017, **5**, 360-368.
22 K. M. Dean, A. E. Palmer, *Nat. Chem. Biol.* 2014, **10**, 512-523.
23 C. Jing, V. W. Cornish, *Accounts Chem. Res.* 2011, **44**, 784-792.
24 R. Wombacher, V. W. Cornish, *J. Biophotonics* 2011, **4**, 391-402.
25 C.-W. Hsieh, C.-H. Chu, H.-M. Lee, W. Y. Yang, *Sci. Rep.* 2015, **5**, 10376.